High sensitivity of taper-based Mach–Zehnder interferometer embedded in a thinned optical fiber for refractive index sensing

J. Yang,[1] L. Jiang,[1,*] S. Wang,[1] B. Li,[1] M. Wang,[1] H. Xiao,[2] Y. Lu,[3] and H. Tsai[4]

[1]Laser Micro/Nano Fabrication Laboratory, School of Mechanical Engineering, Beijing Institute of Technology, 100081, China

[2]Department of Electrical and Computer Engineering, Missouri University of Science and Technology, Rolla, Missouri 65409, USA

[3]Department of Electrical Engineering, University of Nebraska-Lincoln, Lincoln, Nebraska 68588-0511, USA

[4]Department of Mechanical and Aerospace Engineering, Missouri University of Science and Technology, Rolla, Missouri 65409, USA

*Corresponding author: jianglan@bit.edu.cn

Received 17 May 2011; revised 5 July 2011; accepted 5 July 2011; posted 6 July 2011 (Doc. ID 147625); published 30 September 2011

A taper-based Mach–Zehnder interferometer (MZI) embedded in a thinned optical fiber is demonstrated as a highly sensitive refractive index (RI) sensor. A RI sensitivity of 2210.84 nm/RIU (refractive index unit) is obtained at the external RI of 1.40, which is ten times higher than that of normal taper- and long-period fiber grating (LPFG)-based sensors. The sensitivity can be further improved by decreasing the diameter of the thinned fiber and increasing the interferometer length of the MZI. The proposed MZIs have lower temperature sensitivities compared with normal fiber sensors, which is a desirable merit for RI sensors to reduce the cross sensitivity caused by thermal drift.

OCIS codes: 060.2370, 280.4788, 120.3180, 130.6010.

1. Introduction

Recently, optical fiber refractive index (RI) sensors are being increasingly applied in biomedical, chemical, and industrial processes and in the military fields [1–4]. Many types of optical fiber RI sensors have been reported such as long-period fiber gratings (LPFGs) [5–7], fiber Bragg gratings (FBGs) [8,9], abrupt taper-based Michelson interferometer [10], core-offset attenuator-based fiber sensor [11], and other interesting configurations [12,13]. LPFG-based fiber sensors are robust, but with a low RI sensitivity (25–70 nm/RIU in the RI range of 1.3 to 1.38) and a large cross sensitivity to temperature and bending. Only by etching fiber cladding can FBGs be applied for RI sensing that makes the devices frangible. The Michelson interferometer based on taper or core-offset attenuator has a low reflectivity and the RI sensitivity is relatively low (15–40 nm/RIU in the RI range of 1.3 to 1.38). Photonic crystal fiber RI sensors have attracted interest for their low cross sensitivity to temperature; however, costs are high for photonic crystal fiber devices. In recent years, femtosecond lasers have presented unique advantages in 3D structuring of transparent materials [14–16], especially for fiber devices such as ultrasensitive and compact optical fiber sensors [17,18]. Yet, the process is time consuming and complicated with high costs.

Previous works on taper-based Mach–Zehnder interferometer (MZI) devices have been extensively studied, which pertain to power couplers, filters, and sensors [19–22]. However, the sensitivity of this

0003-6935/11/285503-05$15.00/0

normal taper-based MZI without etching for RI sensing is very low (15–40 nm/RIU in the RI range of 1.3 to 1.38). The big cross sensitivity to temperature is also not overcome since the fiber is still a normal fiber.

In this paper, an in-line taper-based MZI embedded in a thinned fiber as a highly sensitive refractive index sensor is proposed. The procedure of fabrication is relatively complicated as compared with normal taper-based fiber sensors. However, this sensor exhibits ten times higher RI sensitivity than normal taper- and LPFG-based fiber sensors. A high sensitivity of 2210.84 nm/RIU (refractive index unit) is achieved in the external RI range of 1.3997–1.4096. It indicates a detection limit of $\sim 4.523 \times 10^{-7}$ at the RI of ~1.4 can be achieved for an optical spectrum analyzer (OSA) with the resolution of the 1 pm. Also, temperature performances of these interferometers are characterized both in atmosphere and water. The sensitivity of an interferometer in atmosphere is as low as 5.94 pm/°C and that in water is −6.66 pm/°C, which is a desirable merit for thermally stable RI sensors.

2. Fabrication and Principle

A. Fabrication

The schematic diagram of the proposed taper-based MZI is shown in Fig. 1(a). A fiber-taper machine (Shanghai Fushuo Inc.) is used to make a long and uniform flat fiber taper as a thinned fiber. About 25 mm fiber coating of the single-mode fiber (Corning SMF-28) is removed and this part is placed right under the flame. The velocity of the hydrogen flow decreases from 170 sccm to 135 sccm and the stretching velocity decreases from 90 μm/s to 45 μm/s when the stretched length (L_{str}) is from 0 to 7 mm in order to get a uniform flat taper with low loss. When the stretched length is larger than 7 mm, the intensity of the flame and the stretching velocity are kept constant. Figure 1(b) shows the microscopic image of a flat taper (a thinned fiber) with a waist diameter of 35 μm. A conventional fusion splicer (model IFS-9, INNO INSTRUMENT, Inc.) is then employed to make a pair of abrupt tapers by electric arc-discharge on the thinned fiber. The arc power and arc time are 8% and 150 ms, respectively. Figure 1(c) is the

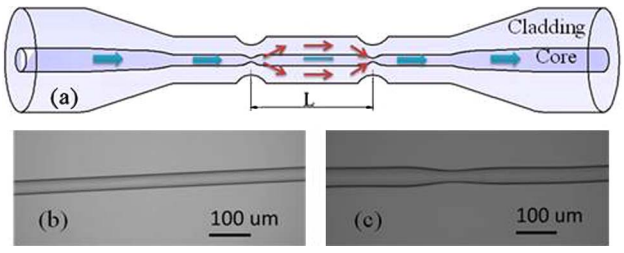

Fig. 1. (Color online) (a) Schematic diagram of the MZI embedded in a thinned optical fiber, (b) the microscopic image of a flat taper (thinned fiber) with a waist diameter of 35 μm, and (c) the microscopic image of an abrupt taper on the thinned fiber with waist diameter (d_1) and length (l_1) of 33 μm and 372 μm, respectively.

Table 1. Parameters of the Interferometers

MZIs	Stretched Length (L_{str}: mm)	Diameter of the Thinned Fiber (D: μm)	MZI length (L_{MZ}: mm)	Waist Diameter of Abrupt Taper 1 (d_1: μm)	Waist Diameter of Abrupt Taper 2 (d_2: μm)
MZI-1	5	56	4	45	49
MZI-2	8	35	4	33	30
MZI-3	8	35	5	34	31

microscopic image of an abrupt taper on the thinned fiber with waist diameter (d_1) and length (l_1) of 33 μm and 372 μm, respectively. Three interferometers are fabricated for comparison and the parameters of them are shown in Table 1.

One end of the interferometer is connected to a tunable laser (Agilent 81980A) with a scanning range of 1465–1575 nm. The other end is connected to an OSA, Agilent 81636B to record the transmission spectrum. The transmission spectra of MZI-1, MZI-2 and MZI-3 are shown in Figs. 2–4, respectively. The transmission losses of the flat tapers (thinned fibers) are only about 0.06 dB, 0.6 dB, and 0.6 dB as shown in Figs. 2(a), 3(a), and 4(a) when their parameters are ($L_{str} = 5$ mm, $D = 56$ μm), ($L_{str} = 8$ mm, $D = 35$ μm), ($L_{str} = 8$ mm, and $D = 35$ μm), respectively. However, when an abrupt taper is added by electric arc-discharge, insertion losses of about 18 dB, 19 dB, and 22 dB are introduced for MZI-1, MZI-2, and MZI-3, respectively. The maximum extinction ratio of MZI-2 is about 20 dB. The fact that the two abrupt tapers in the thinned fiber are not identical to each other leads to the irregular fluctuations in the transmission spectra of the interferometers.

B. Principle

The transmission loss is about 0.06 dB or 0.6 dB when the fiber is tapered to a thinned fiber. Also, the transmission spectrum of the thinned fiber is almost flat across the whole wavelength window. Thus,

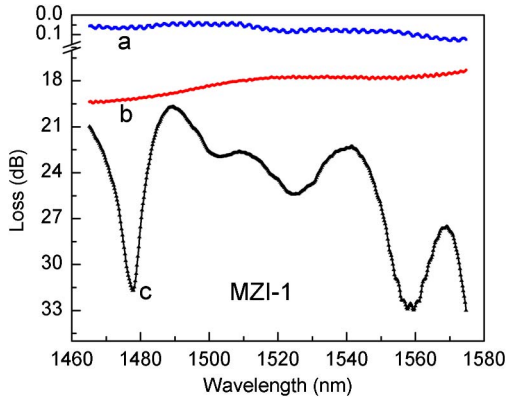

Fig. 2. (Color online) Transmission spectra of (a) the flat taper (thinned fiber), (b) a single abrupt taper embedded in the thinned fiber, and (c) two abrupt tapers embedded in the thinned fiber (MZI-1).

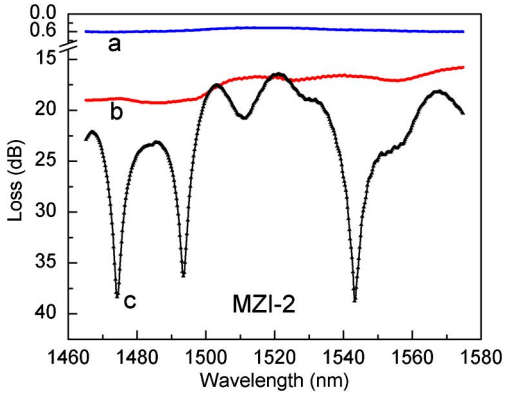

Fig. 3. (Color online) Transmission spectra of (a) the flat taper (thinned fiber), (b) a single abrupt taper embedded in the thinned fiber, and (c) two abrupt tapers embedded in the thinned fiber (MZI-2).

the energy is mainly confined in the thinned core and there is no energy of cladding modes coupling back to the thinned core. But it can be different when two abrupt tapers are introduced in the thinned fiber. When the fundamental mode in the core propagates along the thinned fiber into the first abrupt taper, many cladding modes with different effective refractive indexes can be excited and the left energy keeps propagating forward in the core. These cladding modes are recoupled back into the core when there is a similar abrupt taper within a few millimeters (L_{MZ}) to the first one and they will interfere with each other. The interference between the modes is then expressed as [23]

$$I = \sum_{i=1}^{n} I_i + \sum_{i=1}^{n-1} \sum_{j=i+1}^{n} 2\sqrt{I_i I_j} \cos\left(\frac{2\pi(n_i - n_j)L_{MZ}}{\lambda}\right), \tag{1}$$

where I_i and I_j are the power distributed in the ith order and jth order modes, respectively. n_i and n_j are the effective refractive indices of two interference

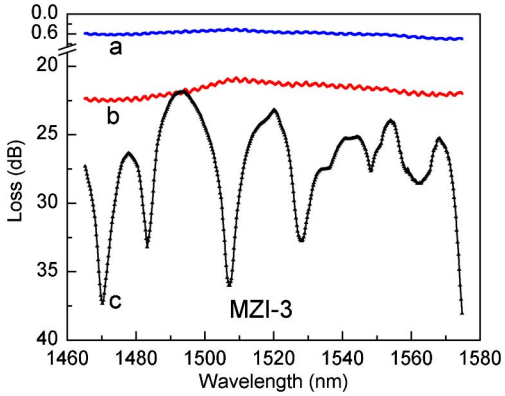

Fig. 4. (Color online) Transmission spectra of (a) the flat taper (thinned fiber), (b) a single abrupt taper embedded in the thinned fiber, and (c) two abrupt tapers embedded in the thinned fiber (MZI-3).

modes, respectively. L_{MZ} is the distance between the two abrupt tapers; λ is the light wavelength in vacuum. The condition for a constructive interference between the modes can be given by $2\pi(n_i - n_j)L_{MZ}/\lambda = 2\pi N$, $(N = 1, 2, 3\ldots)$. The interference pattern of the interferometer is determined by all the modes that match the aforementioned interference condition. Thus nonhomogeneous spectra are seen in Figs. 2–4.

Though there are more than two modes involved in the interference, the energy is mainly distributed in the fundamental mode and one or two cladding modes. Thus, it is reasonable to consider only two main modes to qualitatively analyze the performance of the interferometer to external RI. Since the effective indices of the cladding modes depend on the external RI and that of core mode is independent to external RI, the function of the attenuation wavelength shift with variation of external RI is then approximated as [24]

$$\frac{d\lambda_m}{dn_{ext}} = \frac{-2\pi L_{MZ}}{(2m+1)\pi}\left(\frac{\partial n_j}{\partial n_{ext}}\right) \Big/ \left[1 - \frac{\lambda_m}{\Delta n_{eff}}\left(\frac{\partial n_{co}}{\partial \lambda} - \frac{\partial n_j}{\partial \lambda}\right)\right], \tag{2}$$

where λ_m is the wavelength of attenuation maxima and m is an integer; n_{ext} is the RI of the external medium, and n_{co} is the effective index of core mode (fundamental mode); Δn_{eff} is the effective RI difference between the core mode and the jth cladding mode.

3. Measurement and Discussion

The RI measurement of the fiber sensors are carried out in a clean room with almost constant temperature in order to eliminate the effect caused by temperature fluctuations. The interferometer is taped on a microscope glass slide for shift. It is picked up when applied for RI testing. The ends of the interferometer are held by fiber holders to keep upright. The test sample solution is put on a microscope glass slide, which is supported by a stage right under the interferometer. The height of the stage is carefully adjusted to make sure that the MZI is totally immersed in the solution during the measurement. After each measurement, the stage is lowered and the solution is removed. The glass and the interferometer are cleaned with distilled water and dried by a hairdryer. When a different RI solution is tested, the whole procedure is repeated. Thus, the fiber sensor is kept stationary in the testing process to avoid breakdowns.

Sucrose solutions are tested with different mass concentrations from 0–50% in an interval of 5%. The corresponding RIs are 1.333, 1.3403, 1.3479, 1.3557, 1.3639, 1.3723, 1.3811, 1.3902, 1.3997, 1.4096, and 1.42, respectively. The attenuation wavelength shifts of MZI-1, MZI-2, and MZI-3 are recorded with the increasing of external RI as shown in Fig. 5. The inset in Fig. 5 is the transmission spectra of MZI-1 in different sucrose solutions.

The attenuation peak of interest of MZI-3 is moved out of the wavelength scanning range when

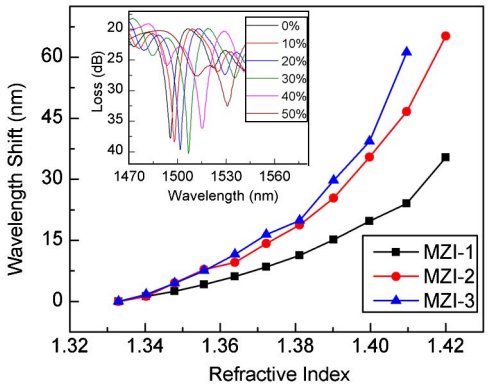

Fig. 5. (Color online) Attenuation wavelength shifts of MZI-1 (squares), MZI-2 (circles) and MZI-3 (triangles) with the increasing of external RI. The inset is the transmission spectra of MZI-1 in different sucrose solutions.

the concentration of sucrose is up to 50%. The sensitivities of MZI-1, MZI-2, and MZI-3 in the RI range of 1.333–1.3811 by linear fitting are 232.9 nm/RIU, 390 nm/RIU, and 430.2 nm/RIU, respectively. The highest sensitivity of MZI-3 is 2210.84 nm/RIU in the RI range of 1.3997–1.4096, and that of MZI-1 and MZI-2 are 1090 nm/RIU and 1786 nm/RIU in the RI range of 1.4096–1.42, respectively. Thus a detection limit of 4.523×10^{-7} can be achieved by MZI-3 near the external RI of 1.40 considering 1 pm resolution of the OSA. According to Fig. 5, the following conclusions can be made: (i) the MZI with longer interferometer length (L_{MZ}) has higher sensitivity; (ii) the sensitivities to external RI of the MZIs are tens of higher than normal taper-based [10,21,22] and LPFG-based [5–7] devices in the same range of RI; and (iii) the MZI embedded in a thinned fiber with smaller diameter (i.e. longer stretched length) have larger sensitivities than that in a bigger thinned fiber.

The conclusion (i) is obvious as RI sensitivity is proportional to interferometer length L_{MZ} as shown in Eq. (2). Note that the attenuation peaks shift to longer wavelengths with the external RI increasing, which is different with those previously reported normal taper-based [10,21,22] and LPFG-based [5–7] sensors. The reason is that $d\lambda_m/dn_{ext}$ in Eq. (2) is different for different cladding modes. A similar mechanism is demonstrated in sensitivity characteristic of LPFGs, where $d\lambda_m/dn_{ext}$ is negative for lower order cladding modes and positive for higher order cladding modes [25]. As for our MZIs, higher order cladding modes are excited in the measured wavelength range and satisfy $(\partial n_{co}/\partial\lambda - \partial n_{cl,j}/\partial\lambda) > \Delta n_{eff}/\lambda_m$ as one can see in Eq. (2). The sensitivity is rather greater for higher order cladding modes as illustrated in [25], thus the conclusion (ii) is demonstrated. The higher order cladding modes can be excited with smaller fiber cladding radius and hence the higher sensitivity can be achieved as described in conclusion (iii). The mechanism is similar with that of LPFGs [26].

In addition, the temperature dependence of the proposed MZIs is tested both in atmosphere and water. The attenuation wavelength shifts of MZI-1 and MZI-2 with increasing of temperature from 50 °C to 300 °C in atmosphere are shown in Fig. 6(a) and the sensitivities are 9.42 pm/°C and 5.94 pm/°C by linear fitting, respectively. The latter is only a ninth of untapered fiber sensors [6,7,17]. The attenuation wavelength shift of MZI-3 with temperature increasing from 30 °C to 70 °C in water is shown in Fig. 6(b) and the sensitivity is −6.66 pm/°C by linear fitting. The low temperature sensitivity in atmosphere can be explained as follows: the concentration of Ge dopant in core is greatly lowered as the fiber is stretched, thus their dependence on temperature is close to that of pure silica fibers which have much smaller temperature sensitivity than Ge-doped fibers [27]. The reason for negative temperature sensitivity of MZI-3 in water is explained as follows: the wavelength blueshifts, because of positive RI sensitivity of the MZIs, is induced by the RI decrease of water with the temperature increases as the temperature RI coefficient of the water is in the order of -10^{-4}/°C [4]. Yet, simultaneously, the wavelength will have redshifts due to increase of RI difference between fiber core and cladding caused by temperature increases. Thus, the performance of the MZI to temperature in water is a combination of the two aspects. As the MZI is sensitive to external RI and

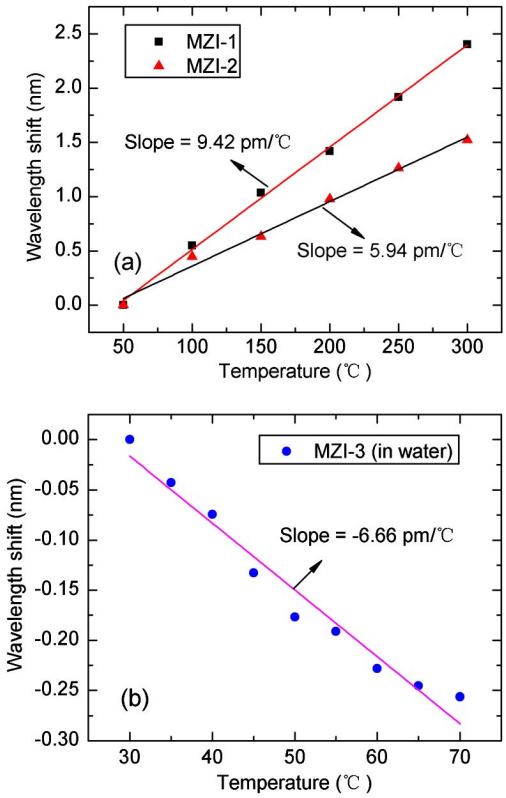

Fig. 6. (Color online) (a) Attenuation wavelength shifts of MZI-1 (squares) and MZI-2 (triangles) with the increasing of temperature in atmosphere. (b) The attenuation wavelength shifts of MZI-3 (circles) with the increasing of temperature in water.

insensitive to temperature in atmosphere, the wavelength blueshift caused by RI decrease of water is slightly larger than the redshift caused by increase of RI difference between fiber core and cladding with temperature increases. Thus, a negative slope of MZI-3 for the temperature test in water is obtained. The lower temperature sensitivity is a desirable merit for RI sensors to decrease the cross sensitivity introduced by temperature change.

4. Conclusions

Taper-based MZIs embedded in thinned optical fibers are fabricated and applied for RI sensing. It is found that (i) the MZI with longer interferometer length has higher sensitivity; (ii) the RI sensitivities of the MZIs are ten times higher than normal taper- and LPFG-based devices in the same range of RI, the highest sensitivity to external RI is 2210.84 nm/RIU around the RI of 1.4; (iii) the sensitivity of the MZI embedded in a smaller diameter thinned fiber is higher than that in a bigger one; and (iv) the proposed MZI has a very low temperature sensitivity, which is a desirable merit for an RI sensor because of the cross sensitivity to temperature.

This research is supported by the National Basic Research Program of China (973 Program) (grant 2011CB013000) and the National Natural Science Foundation of China (NSFC) (grants 90923 039 and 51 025 521).

References

1. J. Zhang, X. Tang, J. Dong, T. Wei, and H. Xiao, "Zeolite thin film-coated long period fiber grating sensor for measuring trace chemical," Opt. Express **16**, 8317–8323 (2008).
2. N. Lin, L. Jiang, S. Wang, L. Yuan, H. Xiao, Y. Lu, and H. L. Tsai, "Ultrasensitive chemical sensors based on whispering gallery modes in a microsphere coated with zeolite," Appl. Opt. **49**, 6463–6471 (2010).
3. N. Lin, L. Jiang, S. Wang, H. Xiao, Y. Lu, and H. L. Tsai, "Thermostable refractive index sensors based on whispering gallery modes in a microsphere coated with poly(methyl methacrylate)," Appl. Opt. **50**, 992–998 (2011).
4. Y. Wang, M. Yang, D. N. Wang, S. Liu, and P. Lu, "Fiber in-line Mach–Zehnder interferometer fabricated by femtosecond laser micromachining for refractive index measurement with high sensitivity," J. Opt. Soc. Am. B **27**, 370–374 (2010).
5. J. F. Ding, A. P. Zhang, L. Y. Shao, J. H. Yan, and S. He, "Fiber-taper seeded long-period grating pair as a highly sensitive refractive-index sensor," IEEE Photon. Technol. Lett. **17**, 1247–1249 (2005).
6. V. Bhatia and A. M. Vengsarkar, "Optical fiber long-period grating sensors," Opt. Lett. **21**, 692–694 (1996).
7. X. Chen, K. Zhou, L. Zhang, and I. Bennion, "Simultaneous measurement of temperature and external refractive index by use of a hybrid grating in D fiber with enhanced sensitivity by HF etching," Appl. Opt. **44**, 178–182 (2005).
8. A. Iadicicco, A. Cusano, A. Cutolo, R. Bernini, and M. Giordano, "Thinned fiber Bragg gratings as high sensitivity refractive index sensor," IEEE Photon. Technol. Lett. **16**, 1149–1151 (2004).
9. X. Fang, C. R. Liao, and D. N. Wang, "Femtosecond laser fabricated fiber Bragg grating in microfiber for refractive index sensing," Opt. Lett. **35**, 1007–1009 (2010).
10. Z. B. Tian, S. S.-H. Yam, and H. P. Loock, "Refractive index sensor based on an abrupt taper Michelson interferometer in a single-mode fiber," Opt. Lett. **33**, 1105–1107 (2008).
11. Z. B. Tian, S. S.-H. Yam, and H. P. Loock, "Single-mode fiber refractive index sensor based on core-offset attenuators," IEEE Photon. Technol. Lett. **20**, 1387–1389 (2008).
12. D. Monzón-Hernández, V. P. Minkovich, J. Villatoro, M. P. Kreuzer, and G. Badenes, "Photonic crystal fiber microtaper supporting two selective higher-order modes with high sensitivity to gas molecules," Appl. Phys. Lett. **93**, 081106 (2008).
13. R. Jha, J. Villatoro, G. Badenes, and V. Pruneri, "Refractometry based on a photonic crystal fiber interferometer," Opt. Lett. **34**, 617–619 (2009).
14. C. H. Lin, L. Jiang, Y. H. Chai, H. Xiao, S. J. Chen, and H. L. Tsai, "Fabrication of microlens arrays in photosensitive glass by femtosecond laser direct writing," Appl. Phys. A **97**, 751–757 (2009).
15. C. H. Lin, Z. H. Rao, L. Jiang, W. J. Tsai, P. H. Wu, and H. L. Tsai, "Investigations of femtosecond–nanosecond dual-beam laser ablation of dielectrics," Opt. Lett. **35**, 2490–2492 (2010).
16. C. H. Lin, L. Jiang, H. Xiao, Y. H. Chai, S. J. Chen, and H. L. Tsai, "Fabry–Perot interferometer embedded in a glass chip fabricated by femtosecond laser," Opt. Lett. **34**, 2408–2410 (2009).
17. L. Zhao, L. Jiang, S. Wang, H. Xiao, Y. Lu, and H. L. Tsai, "A high-quality Mach–Zehnder interferometer fiber sensor by femtosecond laser one-step processing," Sensors **11**, 54–61 (2010).
18. Y. Wang, D. N. Wang, M. Yang, W. Hong, and P. Lu, "Refractive index sensor based on a microhole in single-mode fiber created by the use of femtosecond laser micromachining," Opt. Lett. **34**, 3328–3330 (2009).
19. N. K. Chen and Z. Z. Feng, "Effect of gain-dependent phase shift for tunable abrupt-tapered Mach–Zehnder interferometers," Opt. Lett. **35**, 2109–2111 (2010).
20. X. Z. Wang, Y. Li, and X. Y. Bao, "C- and L-band tunable fiber ring laser using a two-taper Mach–Zehnder interferometer filter," Opt. Lett. **35**, 3354–3356 (2010).
21. P. Lu, L. Men, K. Sooley, and Q. Chen, "Tapered fiber Mach–Zehnder interferometer for simultaneous measurement of refractive index and temperature," Appl. Phys. Lett. **94**, 131110 (2009).
22. Z. B. Tian, S. S.-H. Yam, J. Barnes, W. Bock, P. Greig, J. M. Fraser, H.-P. Loock, and R. D. Oleschuk, "Refractive index sensing with Mach–Zehnder interferometer based on concatenating two single-mode fiber tapers," IEEE Photon. Technol. Lett. **20**, 626–628 (2008).
23. B. Dong, L. Wei, and D. P. Zhou, "Coupling between the small-core-diameter dispersion compensation fiber and single-mode fiber and its applications in fiber lasers," J. Lightwave Technol. **28**, 1363–1367 (2010).
24. B. B. Gu, M. J. Yin, A. P. Zhang, J. W. Qian, and S. He, "Low-cost high-performance fiber-optic pH sensor based on thin-core fiber modal interferometer," Opt. Express **17**, 22296–22302 (2009).
25. X. Shu, L. Zhang, and I. Bennion, "Sensitivity characteristics of long-period fiber gratings," J. Lightwave Technol. **20**, 255–266 (2002).
26. K. S. Chiang, Y. Q. Liu, M. Nar Ng, and X. Y. Dong, "Analysis of etched long-period fiber grating and its response to external refractive index," Electron. Lett. **36**, 966–967 (2000).
27. Y. P. Wang, L. M. Xiao, D. N. Wang, and W. Jin, "Highly sensitive long-period fiber-grating strain sensor with low temperature sensitivity," Opt. Lett. **31**, 3414–3416 (2006).